23rd International Conference
ENGINEERING MECHANICS 2017
Svratka, Czech Republic, 15 – 18 May 2017

STRUCTURAL MODELLING OF THE STRENGTH PROPERTIES OF POLYMER COMPOSITES

R. Chatys*, G. Miśków, J. Miśków*****

Abstract: *This paper analyses the relationship between the structural complexity and the strength properties of fibrous composite materials fabricated by vacuum bag moulding. It shows that the mathematical model based on the critical volume fraction provides relatively good results. The materials under study were three- and five-layer sandwich-structured composites. Composite A consisted of a fibreglass core and two carbon fibre fabric skins. In composite B there was a polyester core between two fibreglass layers and two carbon fibre fabric skins. The results obtained for the materials suggest that this method can be used by design engineers working with a wide variety of polymer composites.*

Keywords: Composite, Strength properties, Critical volume fraction, Vacuum bag, Modelling.

1. Introduction

The development of new composites, e.g. sandwich-structured composites, with specific properties different from those of traditional structural materials, has led to an increased interest in polymer-matrix composite materials. The materials have a wide range of potential applications. They are particularly suitable where innovative solutions are required. Because of their high strength properties (Reifsnider, 2005 and Chatys, 2013), they can be used in various controlled mobile systems (Stefański et al., 2014), including unmanned aerial vehicles (Gapinski, 2014 and Koruba, 2010), where properties superior to those of traditional structural materials not containing reinforcing particles are necessary. A vital characteristic of composite materials is that their structure can be designed in such a way as to obtain desirable properties to suit the needs of any industry (Pavelko, 2007); hence extensive research is a prerequisite.

2. Description of an executive anti-aircraft missile control element

The model verifying the strength properties of the composites under study assumed that the distribution of stresses in the volume was uniform. The fibre failure was considered using the critical volume fraction (Fig. 1) for components differing in the physical and mechanical properties (Fig. 2) (Paramonov, 2012).

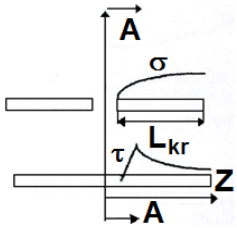

Fig. 1: Transfer of stress to the adjacent reinforcement (Blumbergs et al., 2010) resulting from tangential stress (τ).

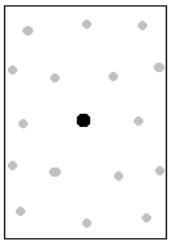

Fig. 2: Volume fraction of the laminate with a damaged fibre (•) (Blumbergs at al., 2010).

* Assistant Prof. Rafał Chatys, Post-doctoral degree Eng.: Faculty of Mechatronics and Mechanical Engineering, Kielce University of Technology, al. 1000-lecia P.P. 7; 25-345, Kielce; PL, chatys@tu.kielce.pl

** Gracjan Miśków, MSc: Phoenix Equipment Polska, ul. Jodłowa 54, 77-200 Miastko; PL, biuro@phoenixequipment.pl

*** Jerzy Miśków, MSc: Bielsko Aviation, Entrepreneurship and Innovation Park, ul. Stefana Kośki 43, 43-512 Kaniów, PL opticup@opticup.com.pl

It is quite difficult to determine the exact location of the damaged fibres (reinforcement) (•) because of their random distribution. Moreover, the damage process increases with increasing load between the fibres. The fibre failure in a composite is connected with the mechanism of distribution of stresses between the neighbouring fibres. The area and volume of this zone are dependent on the ineffective length (*1*) along which the damaged fibre transfers stress to adjacent fibres through tangential stresses (*2*) (Tab. 1).

Tab. 1: Model parameters.

Model parameters	Relationships
ineffective length	$L_{kr} = d_j \left[\left(\frac{1-\nu^{0,5}}{\nu^{0,5}} \right) \cdot \frac{E_f}{G_m} \right]^{0,5} \operatorname{arccos} h \left[\frac{1-(1-\varphi)^2}{2 \cdot (1-\varphi)} \right]$ (1) where: d_f – fibre diameter; ν – fibre volume; E_f – Young's modulus for the fibre; G_m – matrix shear modulus; φ –level of interaction between the reinforcement and the matrix (φ = 0.97 %).
tangential stress	$\tau_{lok} = \frac{\beta r}{2} \cdot \varepsilon E_i \tanh\left(\frac{\beta l}{2} \right)$ (2) where: β – const. (β = 1 / B); r – fibre radius; ε – elongation; l – fibre length (critical length).
maximum stress	$\sigma_{\max} = \frac{2\tau_{lok}}{\beta r} \left[\frac{1}{\tanh\left(\frac{\beta l}{2} \right)} - \frac{1}{\sinh\left(\frac{\beta l}{2} \right)} \right]$ (3) where: β –const. (β = 1 / B); r –fibre radius; l –fibre length (critical length); τ_{lok} –tangential stress.

The failure process continues since the loading of the fibre increases by the value of stress transferred from the damaged fibre. The ultimate tensile strength of the laminate (fibre bundles) is exceeded, which leads to a redistribution of the local stresses τ_{lok} in the adjacent components. If the stress is lower than the ultimate tensile stress, the volume fraction will continue to transfer stresses to the adjacent fibres. Knowing the tangential stress of the i-th volume fraction, we can calculate the maximum stress (σ_{max}) in the damaged area. Its lowest value will indicate the strength of the composite.

3. Materials and methods

The sandwich-structured composites fabricated by vacuum bagging consisted of a polymer reinforcement in the form of fibreglass fabric [0 ° / -90 °] (Fig. 3a) and Rymatex biaxal carbon woven cloth (Fig. 3b) with a basis weight of 600 g/m^2 and 400 g/m^2, respectively. The vacuum bag moulding process involved using vacuum pressure generated in the closed mould to press the laminate components (Paramonov et al., 2012). Before the gelcoat - a resin/hardener mixture - was applied, the reinforcement layers were degreased with Spacewax 300 wax and the mould surface was polished (Fig. 3d) to make the separation of the cured composite easier. Then, the mould edges were covered with double-sided tape to which a flexible bag was attached in order to ensure that the system was well-sealed and constant vacuum pressure could be maintained throughout the process.

a) *b)* *c)* *d)* *e)* *f)* *g)* *h)* *i)* *j)*

Fig. 3: Stages of fabrication of composite A and composite B.

The next stage required coating the mould with a first layer of epoxy resin (Fig. 3e). The resin-to-hardener ratio was 3-to-1 (100 g of LH 289 resin to 33 g of L 289 hardener), as recommended in the operation sheet. In composite A there were three layers: two carbon fibre fabric skins and fibreglass as the core material (Fig. 3f). The surface of the laminate was wet out with epoxy resin (Fig. 3g). Composite B

was formed in a similar way but the core material was Lantor Coremat®) Soric XF (Fig. 3c), which is characterised by high resin absorption when impregnated. The honeycomb plate (Fig. 3h) was placed in between two layers of resin-soaked fibreglass fabric (Fig. 3i) with carbon fibre fabric skin (Fig. 3j) on both sides. The top layer was also wetted with epoxy resin. The other materials required to complete the vacuum system and assist in the laminating process included peel ply (release fabric), breather fabric and perforated film. A control valve was incorporated in the breather fabric to control the volume of vacuum pressure in the envelope. The air was removed from the system through a flexible hose connected to a vacuum pump. The laminating process was completed at a pressure of -0.9 bars. The materials were heat treated at a temperature of 600 ºC for 5.5 hours. The sandwich panels fabricated at the Laboratory of Composite Materials of the Kielce University of Technology were cut into testpieces with dimensions specified in the PN-EN 10002-1+ACI standard using an A.P.W2010BB waterjet cutting system (Nowakowski, 2016). Composite A and composite B were cut with a speed of 2.0 and 0.8 m/s, respectively. The next stage was quasi-static tensile tests carried out on composite A specimens in accordance with the ISO 14129:1997 standard; the experimental data were obtained using an INSTON 8501 universal testing machine operating at a speed of 2 mm/min. Composite B in the form of unnotched specimens with dimensions of 100 x 10 x 3 mm was tested to determine its Charpy impact resistance in accordance with the PN-EN ISO 179-2 standard using an Instron CEAST 9050 impact pendulum with an energy of 25 J.

4. Results and discussion

The strength parameters obtained for composite A were characterised by a slight scatter of results with an average of 537.30 MPa (Tab. 2). The three-ply composite failed by shear at the interphase boundary and the resin layer containing the fibreglass fabric between the two carbon fibre layers, which was due to the occurrence of defects in the laminate structure and the cutting parameters applied during cutting.

Tab. 2: Mechanical properties of composite A fabricated by vacuum bagging.

Specimen number	F_{max} [N]	ε [mm]	σ_{max} [MPa]	E [MPa]
A1	1197.5	1.44	532	4.9
A2	1286.0	1.68	542	5.0
A3	1208.0	1.38	538	4.9
Average value	**1230.5**	**1.50**	**537.30**	**4.93**

The modelled values of strength (failure at the lowest volume fraction) in composite A and composite B (with the Soric XF core) were found to be 612.60 and 552.48 MPa, respectively (Tab. 3). The experimental value of σ_{max} reported for composite A was 20 % lower than the modelled value. The structural complexity and a larger number of defects in the structure (scale effect) of composite B resulted in a greater decrease in the modelled value of σ_{max} (of about 10 %).

Tab. 3: Modelled parameters of the sandwich-structured composites.

Material	L_{kr} [mm]	τ_{lok} [MPa]	σ_{max} [MPa]
Composite A	0.590	6.047	612.60
Composite B	0.494	5.938	552.48

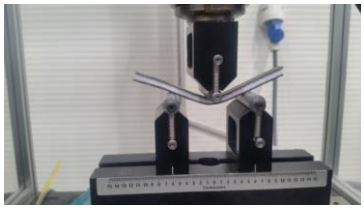

Fig. 4. Specimen under three-point bending.

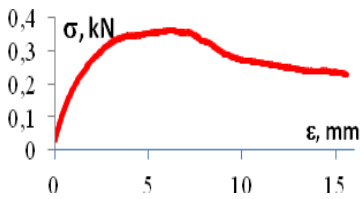

Fig. 5. Load vs. elongation for composite B.

The modifications to the structure of composite A aimed at extending its use in lightweight load-carrying structures. The laminate was modified by adding a polyester core in between the fibreglass reinforcement and carbon fibre skins (composite B). The results obtained for composite B during the three-point

bending tests (Fig. 4) were used to determine the adhesive strength at the interface between the carbon fibre and glassfibre reinforcement and the polyester core (Fig. 5). The analysis of the $\sigma - \varepsilon$ relationship revealed that it was a ductile material because the curve had no clear yield point at which adhesion at the interface between the core and the glass and carbon reinforcement failed. Apart from the three-point bending test, composite B was subjected to impact loading, which lightweight load-carrying structures may be exposed to. The results of the impact resistance tests (R_e) for composite B with a honeycomb core showed that there was a fracture (delamination) of the core with separation of the reinforcement from the core on one side. The average value of the impact resistance of composite B obtained from three tests was 133.75 kJ/m^2 (Tab. 4).

Tab. 4: Impact resistance of composite B.

Specimen number	**Specimen dimensions**	**R_e [kJ/m^2]**
B1	120 x 10.5 x 7.8	137.99
B2		130.58
B3		132.68
Average value	**120 x 10.5 x 7.8**	**133.75**

5. Conclusions

The strength properties of polymer composites with different arrangements of their constituents to be used in different applications are analysed using various tests and calculation methods, which help estimate more or less approximately these parameters for a designed structure. This paper has discussed two materials that can be used in structures where light weight and high strength are required. When a new material is approved (and certified) for a specific use, calculation and simulation results are not taken into account. However, structural engineers involved in design rely on data obtained from methods of estimation. This paper has dealt with experiments on composite materials with specifically arranged fibres, which exhibits different strength properties. The inaccuracy of the common calculation methods used to determine the strength of composite structures is due to the quality of the lamination process (Chatys, 2013). Composite materials fabricated by vacuum bag moulding are very compacted; bundles of continuous fibres (differing in weight) are arranged into arrays according to the number and stacking sequence of layers where stress concentrations are present.

References

Chatys, R. (2013) Investigation of the Effect of Distribution of the Static Strength on the Fatigue Failure of a Layered Composite by Using the Markov Chains Theory. Mechanics of Comp. Materials, 48, 6, pp. 629-63.

Blumbergs, I., Chatys, R. and Kleinhofs, M. (2010) Experimental Research of Carbon Fiber Composite Material Characteristics. Proc. Of IV Int. Conf. on Scientific Aspects of Unmanned Aerial Vehicle – SAUAV'2010", May, 5-7, Suchedniów, Poland, pp. 46-51.

Gapinski, D. and Krzysztofik, I. (2014) The process of tracking an air target by the designed scanning and tracking seeker, in: Proc. 2014 15th Int. Carpathian Control Conf. (eds. Petras, I., Podlubny, I., Kacur, J., and Farana, R.), IEEE, pp. 129-134.

Koruba, Z., Dziopa, Z. and Krzysztofik, I. (2010) An analysis of the gyroscope dynamics of an anti-aircraft missile launched from a mobile platform. Bulletin of the Polish Academy of Sciences – Technical Sciences, 58, 4, pp. 651-656.

Nowakowski, L. and Wijas, M. (2016) The evaluation of the process of surface regeneration after laser cladding and face milling, in: Proc. 22th Int. Conf. Eng. Mech. 2016 (eds. Zolotarev, I. and Radolf, V.), Inst. Thermomechanics, Acad. Sci. Czech Republic, Prague, pp. 430-433.

Paramonov, J., Chatys, R., Anderson, J. and Kleinhofs, M. (2012) Markov Model of Fatigue of a Composite Material with Poisson Process of Defect Initiation, Mechanics of Composite Materials, 48, 2, pp. 217-228.

Pavelko, I., Pavelko, V. and Chatys, R. (2007) Strength of Fibrous Composites with Impact Damage, Journal Mechanika, 219, pp. 187-198.

Reifsnider, K.L. and Stinchcomb, W.W. (2005) A Critical-Element Model of the Residual Strength and Life of Fatigue-Loaded Composite Coupons, Composite Materials: Fatigue and Fracture, Astm stp 907, pp. 298-313.

Stefański, K., Grzyb, M. and Nocoń, Ł. (2014) The analysis of homing of aerial guided bomb on the ground target by means of special method of control, in: Proc. 2014 15th Int. Carpathian Control Conf. (eds. Petras, I., Podlubny, I., Kacur, J., and Farana, R.), IEEE, pp. 551-556.